

Article

Mechanical and Microstructural Response of Iron Ore Tailings under Low and High Pressures Considering a Wide Range of Molding Characteristics

Giovani Jordi Bruschi ^{1,*}, Carolina Pereira Dos Santos ¹, Hugo Carlos Scheuermann Filho ¹,
Camila da Silva Martinatto ¹, Luana Rutz Schulz ¹, João Paulo de Sousa Silva ² and Nilo Cesar Consoli ¹

¹ Graduate Program in Civil Engineering, Universidade Federal do Rio Grande do Sul, Porto Alegre 90035-190, RS, Brazil; camilamartinatto@hotmail.com (C.d.S.M.); consoli@ufrgs.br (N.C.C.)

² Exploration and Mineral Projects—Mineral Development Centre, VALE S.A., BR-381, Santa Luzia 33040-900, MG, Brazil; joao.paulo.silva@vale.com

* Correspondence: gio.bruschi@gmail.com

Abstract: The dry stacking of filtered tailings is an option to deal with safety-related issues involving traditional slurry disposition in impoundments. Filtered tailings can be compacted to pre-define design specifications, which minimizes structural instability problems, such as those related to liquefaction. Yet, comprehending the tailing's response under various stress states is essential to designing any dry stacking facility properly. Thus, the present research evaluated the mechanical response of cemented and uncemented compacted filtered iron ore tailings, considering different molding characteristics related to compaction degree and molding moisture content. Therefore, a series of one-dimensional compression tests and consolidated isotropically drained triaxial tests (CID), using 300 kPa and 3000 kPa effective confining pressures, were carried out for different specimens compacted at various molding characteristics. In addition, changes in gradation owing to both compression and shearing were evaluated using sedimentation with scanning electron microscope tests. The overall results have indicated that the 3% Portland cement addition enhanced the strength and stiffness of the compacted iron ore tailings, considering the lower confining pressure. Nevertheless, the same was not evidenced for the higher confining stress. Moreover, the dry-side molded specimens were initially stiffer, and significant particle breakage did not occur owing to one-dimensional compression but only due to shearing (triaxial condition).

Keywords: iron ore tailings; dry staking; filtered tailings; tailings dam; Portland cement



Citation: Bruschi, G.J.; Santos, C.P.D.; Filho, H.C.S.; da Silva Martinatto, C.; Schulz, L.R.; Silva, J.P.d.S.; Consoli, N.C. Mechanical and Microstructural Response of Iron Ore Tailings under Low and High Pressures Considering a Wide Range of Molding Characteristics. *Mining* **2023**, *3*, 712–730. <https://doi.org/10.3390/mining3040039>

Academic Editors: Mostafa Benzaazoua, Krzysztof Skrzypkowski, René Gómez, Fhatuwani Sengani, Derek B. Apel, Faham Tahmasebinia and Jianhang Chen

Received: 24 August 2023
Revised: 14 November 2023
Accepted: 16 November 2023
Published: 18 November 2023



Copyright: © 2023 by the authors. Licensee MDPI, Basel, Switzerland. This article is an open access article distributed under the terms and conditions of the Creative Commons Attribution (CC BY) license (<https://creativecommons.org/licenses/by/4.0/>).

1. Introduction

The dry stacking of filtered tailings has become feasible due to the recent evolution of dewatering technologies, which enables the obtainment of an unsaturated material, known as ‘cake,’ that can be compacted to form stackings of hundreds of meters [1,2]. Hence, this technique can potentially overcome most safety-related drawbacks associated with traditional slurry disposal in pounds. That is, the stored tailings are no longer found saturated and in a loose condition susceptible to liquefaction. They are arranged according to design specifications, such as dry density and compaction water content [3,4]. In addition, dry stacking requires less physical space for tailings storage. It involves recovering substantial amounts of water that can be later reused in the extraction and beneficiation processes [5].

The dry stacking of mining tailings has become an attractive alternative, especially considering that more rigid regulations/laws have been recently introduced prohibiting the construction of new tailings dams using the upstream method while demanding the de-characterization and decommissioning of existing ones in countries such as Brazil [6]. This was motivated by the recent catastrophic incidents that occurred in the Fundão dam

(2015) and Mina do Córrego do Feijão (2019) dam, both of which stored iron ore tailings and were constructed using the upstream method [7–9]. In this sense, Brazil has been one of the top three global iron ore suppliers, with the Quadrilátero Ferrífero (Iron Quadrangle) region (located in the province of Minas Gerais) accounting for around 65% of the Brazilian iron ore production [10,11]. This scenario highlights the need to reallocate the vast amount of iron ore tailings already stored in upstream dams and provide a proper destination for the upcoming tailings.

The appropriate conception of a tailings storage facility (*TSF*) relies upon comprehending the tailings' mechanics under operational boundary conditions, which involves, among other aspects, knowing the material's response under various stress states [12,13]. In this regard, dry stacking tailings have the advantage over hydraulic disposal in dams concerning spatial predictability of the tailing's properties. The first involves the compaction of a well-characterized material. In contrast, the latter comprehends the hydraulic deposition, sedimentation, and subsequent consolidation over a vast impoundment, enhancing the problem's inherent complexity [14,15]. Still, a resilient design of a dry stacking facility demands an understanding of the filtered tailings response over a wide range of stresses and the effect of the compaction characteristics on the mechanical response. Eventually, it is also possible to incorporate a cementitious material into the tailings to enhance the material's strength and stiffness [16–20].

The behavior of artificially cemented geomaterials is well-known and extensively documented: developing a cementitious matrix in a granular media leads to significant strength and stiffness gains until cementing bond degradation, accompanied by a more dilatative response and post-peak brittleness [21,22]. Naturally, once the bonds are degraded, the cement is ineffective in providing actual enhancements in the material's mechanical response; that is, the cement may be useless for higher confinement levels [23]. In general, artificially cemented tailings behave like cemented soils and can be analyzed using the same approaches [18]. Nonetheless, despite a variety of studies concerning the response of cemented tailings for mine backfill [19,24–29], few have been carried out on the behavior of artificially cemented filtered tailings for dry staking purposes, particularly for high-stress levels and different compaction conditions.

Accordingly, the present study evaluated the mechanical response of cemented ($C = 3\%$) and uncemented ($C = 0\%$) compacted filtered iron ore tailings under low ($p'_0 = 300$ kPa) and high ($p'_0 = 3000$ kPa) confining pressures. Both cemented and uncemented test specimens were molded considering various compaction characteristics that involved compaction degrees (97% and 100%) for modified and standard Proctor compaction efforts and moisture contents (dry, optimum, and wet sides of the compaction curve). A series of 1-D consolidation tests were carried out for all the test specimens and consolidated isotropically drained triaxial tests (*CID*) under two different confinement levels ($p'_0 = 300$ kPa and $p'_0 = 3000$ kPa). Particle breakage analysis was carried out for both stress paths with sedimentation and scanning electron microscope tests.

2. Experimental Program

Three phases compose the experimental program. The first comprehended the physical characterization of the iron ore tailings (*IOTs*), in which the molding points were determined based on the compaction characteristics obtained using the standard and modified Proctor compaction efforts—the second consisted of the conduction of the 1-D compression tests and the triaxial tests, both executed on the cemented and uncemented tailings compacted under different conditions. In the third phase, the possibility of particle breakage during the compression and shearing of the specimens was evaluated using the analysis of grain size distribution with the aid of scanning electron microscope (*SEM*) tests.

3. Materials

The iron ore tailings utilized herein come from a filtration plant in the Province of Minas Gerais (southeast Brazil). Table 1 summarizes the main physical characteristics of these tailings.

Table 1. Physical properties of the iron ore tailings.

Physical Properties	Iron Ore Tailings	Test Method
Liquid limit (%)	-	
Plastic limit (%)	-	ASTM D4318
Plastic index (%)	non-plastic	
Specific gravity	2.72	ASTM D854
Coarse Sand (2.00 mm < diameter < 4.75 mm) (%)	0.0	
Medium Sand (0.425 mm < diameter < 2.00 mm) (%)	0.0	
Fine Sand (0.075 mm < diameter < 0.425 mm) (%)	8.0	ASTM D7928
Silt (0.002 < diameter < 0.075 mm) (%)	88.7	
Clay (diameter < 0.002 mm) (%)	3.3	
Maximum dry unit weight at standard effort (kN/m ³)	17.4 (<i>w</i> = 15.2%)	ASTM D1557
Maximum dry unit weight at modified effort (kN/m ³)	18.5 (<i>w</i> = 11.6%)	ASTM D698

The gradation was evaluated through sedimentation and sieve analysis following ASTM D7928 [30]. The Atterberg limits and the specific gravity were analyzed following ASTM D4318 [31] and ASTM D854 [32], respectively. According to the Unified Soil Classification System [33], the studied IOTs can be classified as silty sand once non-plastic and around 83% of their particles are in the silt-size range. Figure 1 depicts the compaction characteristics obtained using the standard ASTM D698 [34] and the modified ASTM D1557 [35] Proctor compaction efforts.

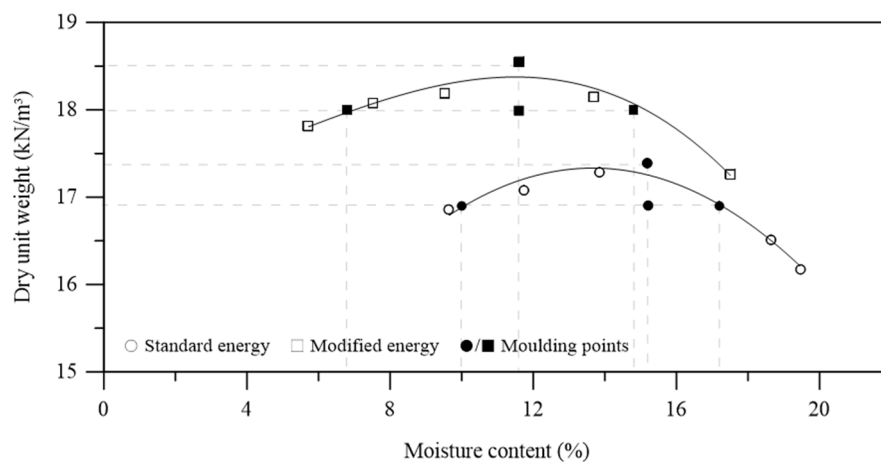
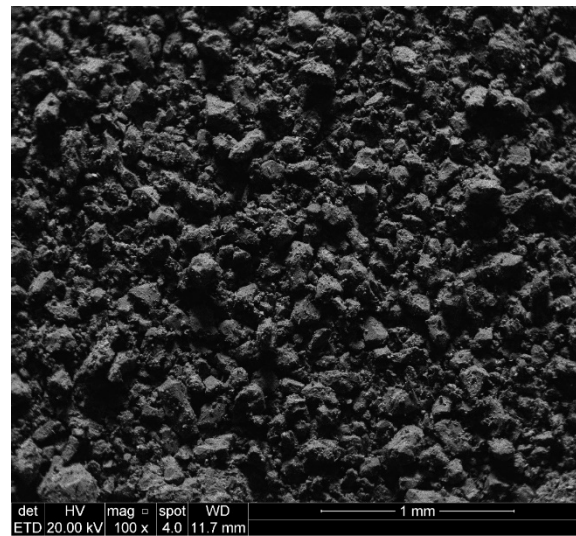
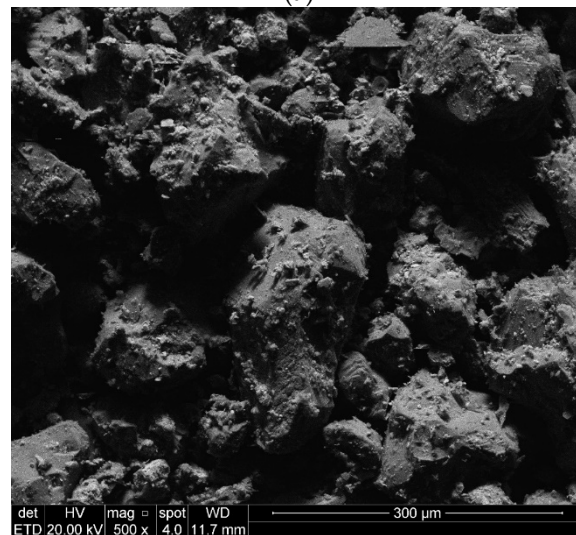


Figure 1. Compaction characteristics of the iron ore tailings and molding points.

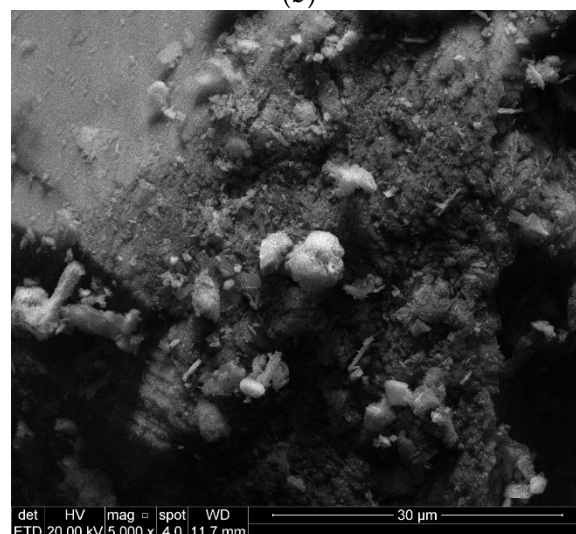
Chemically, the X-ray fluorescence (XRF) test has revealed that the IOTs are mainly constituted of silicon (Si = 57%), iron (Fe = 36%), and aluminum (Al = 5%), as well as other minor constituents. Mineralogically, X-ray diffraction analysis (XRD), combined with a semi-quantification using the reference intensity ratio (RIR) method, have attested the presence of quartz (85%), kaolinite (13%), and hematite (3%). Figure 2 exhibits the scanning electron microscope (SEM) micrographs of the iron ore tailings at 100× (Figure 2a), 500× (Figure 2b), and 5000× (Figure 2c) magnification rates. The IOTs are composed primarily of flattened-angular quartz grains and a lesser amount of smaller hematite particles (Figure 2c).



(a)



(b)



(c)

Figure 2. SEM micrographs of the iron ore tailings magnified by (a) 100 \times and (b) 500 \times ; (c) 5000 \times .

The XRF tests were conducted on a WDS spectrometer model RIX 2000 from Rigaku®. A D-500 Siemens® X-ray diffractometer (Akishima-shi, Tokyo, Japan), equipped with a fixed Cu anode tube, was used in the XRD tests, whereas a scanning electron microscope with an electron beam of 20 kV using gold-coated samples (Q150 and JMS-6610 models) was used for the SEM tests. Commercially available high early strength Portland cement (type III) was used as the cementing agent. The cement's specific grain unit weight was 3.15 g/cm³. Distilled water was used for molding and saturating the test specimens and throughout the physical characterization tests.

4. Methods

4.1. Molding Characteristics

Characteristics of the filtered cake, such as gradation and moisture content, may vary across a particular range owing to inherent variations related to the filtration plant and the tailings' nature [36–38]. As a result, the filtered tailings moisture content (w) is a crucial variable in affecting the compaction process and, thus, the in situ mechanical response of the compacted material, as it is intimately linked to both the attainable compaction degrees and the compacted materials fabrics [39–41]. Therefore, understanding the iron ore tailings response under certain compaction conditions is essential to guarantee a rational design of filtered STF.

Considering the cemented and uncemented specimens, the molding points were based on the compaction tests and are depicted in Figure 1. For both compaction efforts, the highest dry density values and the corresponding optimum moisture contents were chosen. In addition, within each curve, three points with a degree of compaction of around 97% were chosen: one located on the dry side of the curve, one located on the wet side of the curve, and the other presenting the same dry unit weight of those two but molded using the corresponding optimum moisture content. Therefore, those three additional points obtained for each compaction curve have the same molding void ratio but different molding moisture contents. This enables the assessment of the influence of molding characteristics on the response of the cemented and uncemented iron ore tailings.

4.2. Specimen Molding and Curing

Cylindrical specimens were statically molded for the one-dimensional compression tests (5 cm in diameter and 2 cm in height) and the triaxial tests (5 cm in diameter and 10 cm in height). For the first, the material was directly compacted in one layer inside the oedometric ring. For the latter, the compaction was carried out in three layers in a cylindrical split mold, with the top of the first and second layers slightly scarified to guarantee the adherence of the subsequent layer. Still, before compaction, the correct amount of distilled water, iron ore tailings, and cement (when needed) were manually mixed until a homogeneous material of a homogeneous aspect was obtained. For the cemented samples (containing 3% of cement based upon the mass of dry tailings), the oedometric ring or the retrieved specimen from the split mold was sealed inside a plastic bag and forwarded to be cured in a room with a controlled environment (23 ± 2 °C and 95% of relative moisture). All cemented specimens were cured for seven days. Otherwise, the specimens were ready to be tested. As an acceptance criterion, each sample was considered suitable for testing if the following requirements were met: dry unit weight (γ_d) within $\pm 1\%$ of the target value and moisture content (w) within $\pm 0.5\%$ of the assigned value.

4.3. One-Dimensional Compression Tests

The one-dimensional compression tests agreed with the procedures stated by ASTM D2435 [42] using a setup composed of a consolidometer, a load device, and a linear variable differential transformer (LDVT) used to measure the vertical displacement. Porous discs and filter papers were utilized at the bottom and top of the testing ring to permit the drainage of the compacted specimen during the loading stages. After applying a setting

stress of 5 kPa, the loading schedule was: 50 kPa, 100 kPa, 200 kPa, 400 kPa, 800 kPa, 1600 kPa, 3200 kPa, and 6400 kPa.

4.4. Triaxial Tests

Consolidated isotropically drained (CID) triaxial tests were carried out according to the recommendations preconized by ASTM D7181 [43] in a triaxial test apparatus capable of attaining high confining pressures and in which all the data were digitally monitored and recorded. The test samples were entirely saturated by a process involving CO₂ percolation, distilled water percolation, and the increment of backpressure (maintaining $p' = 20$ kPa) at a rate of 1.5 kPa/min. Irrespective of the test specimen configuration, a backpressure of 400 kPa was sufficient to guarantee the obtainment of B values greater than 0.95. The consolidation stage consisted of incrementing the chamber confining pressure at a 2 kPa/min rate up to the desired initial mean effective stress (p'_0) value. At this rate, no excess pore pressure was developed. The shearing followed a conventional loading path, maintaining the confining pressure constant, conducted at a strain rate of 1.0 mm/hour. Hall effect sensors [44], attached directly to the test specimen (two in the axial direction and one in the radial direction), enabled the local strain assessment along all the test phases. Also, the volumetric strains during the consolidation and shearing phases were measured by the flow volume of water leaving/entering the specimen. Both confining pressure and backpressure were digitally monitored by pressure transducers and were applied using general-purpose water pressure sources. The axial load was also digitally scanned using a 100 kN load cell.

4.5. Particle Breakage Analysis

The possibility of particle breakage owing to the one-dimensional consolidation and the shearing phase on the triaxial test was evaluated for some representative specimens. Quantitatively, the after-test gradation was compared to the natural (untested) iron ore tailings grain size distribution using the particle breakage factor (B_f). The breakage factor is defined as the difference between the amount of the finer particles after testing compared to the original content of finer particles [45]. Qualitatively, SEM micrographs were carried out on some specimens to study the particle breakage, as shown in Section 5.3.

5. Results and Discussions

The notation used to characterize a test specimen takes the form of A_B_C. **A** is the corresponding compaction energy (S = standard; M = modified), **B** refers to the molding moisture content relative to the compaction curve depicted in Figure 1 (W = wet side; O = optimum; R = optimum but with reduced density; D = dry side), and **C** concerns the amount of cement required (3C = 3%; 0C = 0%).

5.1. One-Dimensional Compression Tests

Figure 3a depicts the one-dimensional compression tests for the uncemented iron ore tailings specimens, and Figure 3b exhibits the same results, considering the samples containing 3% cement. Initially, the cemented samples were substantially less compressible until cementing bond breakage, which occurred at vertical pressures below 800 kPa.

Table 2 summarizes the values of the compression indexes (C_c). These C_c values indicate that, at higher pressures, the molding void ratio appears to influence the slope of the one-dimensional normal compression line (1D-NCL).

In other words, the C_c values of the denser samples are very similar, as are the C_c values of the looser specimens. Nevertheless, the compression curves converge towards a unique 1D-NCL, indicating that the initial fabric effects created by the cement addition and compaction characteristics would be erased at higher stresses [46]. This is reinforced when calculating the m parameter [47], obtained by plotting a specific volume at the most elevated pressure versus a specific volume at 20 kPa. Considering the test specimens' data, no linear trend was obtained, and the resultant m was close to zero, indicating no

transitional behavior of the studied iron ore tailings [48]. In this regard, at the highest vertical pressure, the difference between the highest and lowest e values was only 0.024.

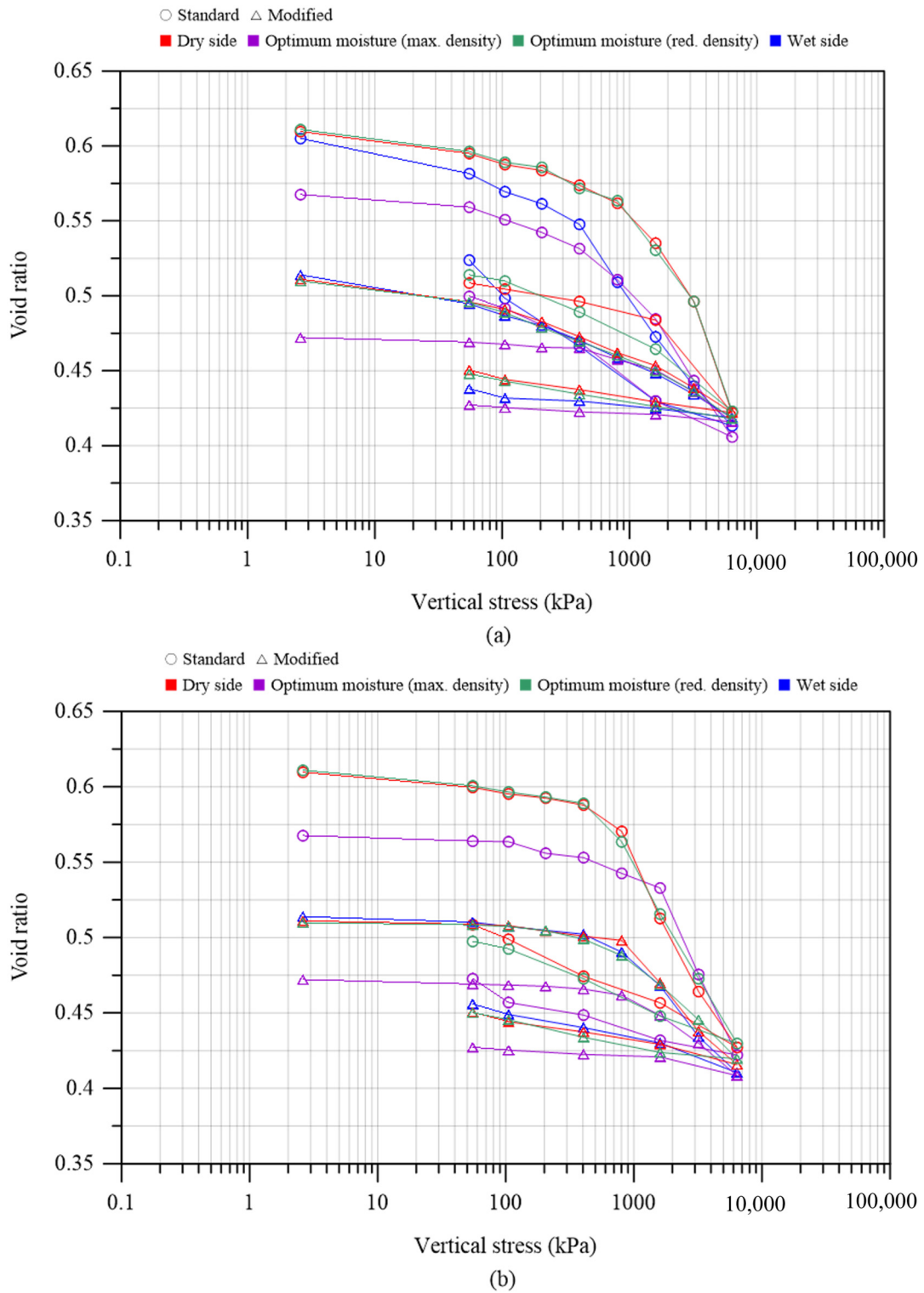


Figure 3. One-dimensional compression tests (a) uncemented and (b) cemented specimens.

Table 2. One-dimensional compression characteristics.

Specimen	e_0	e_{6400}	C_c
S_W_3C	0.605	0.412	0.14
S_O_3C	0.568	0.422	0.14
S_R_3C	0.608	0.428	0.14
S_D_3C	0.610	0.427	0.14
M_W_3C	0.512	0.410	0.10
M_O_3C	0.471	0.408	0.07
M_R_3C	0.511	0.412	0.11
M_D_3C	0.509	0.414	0.10
S_W_0C	0.603	0.412	0.11
S_O_0C	0.566	0.403	0.14
S_R_0C	0.608	0.421	0.12
S_D_0C	0.609	0.421	0.12
M_W_0C	0.512	0.426	0.04
M_O_0C	0.473	0.419	0.04
M_R_0C	0.514	0.421	0.04
M_D_0C	0.514	0.422	0.04

5.2. Triaxial Tests

5.2.1. Stress–Strain Data

The stress–strain ($\epsilon_a \times q$) response and the volume change behavior ($\epsilon_a \times \epsilon_v$) are plotted in Figure 4a ($p'_0 = 300$ kPa, uncemented), Figure 4b ($p'_0 = 300$ kPa, cemented), Figure 4c ($p'_0 = 3000$ kPa, uncemented), and Figure 4d ($p'_0 = 3000$ kPa, cemented). Table 3 summarizes the main data relative to the triaxial testing program.

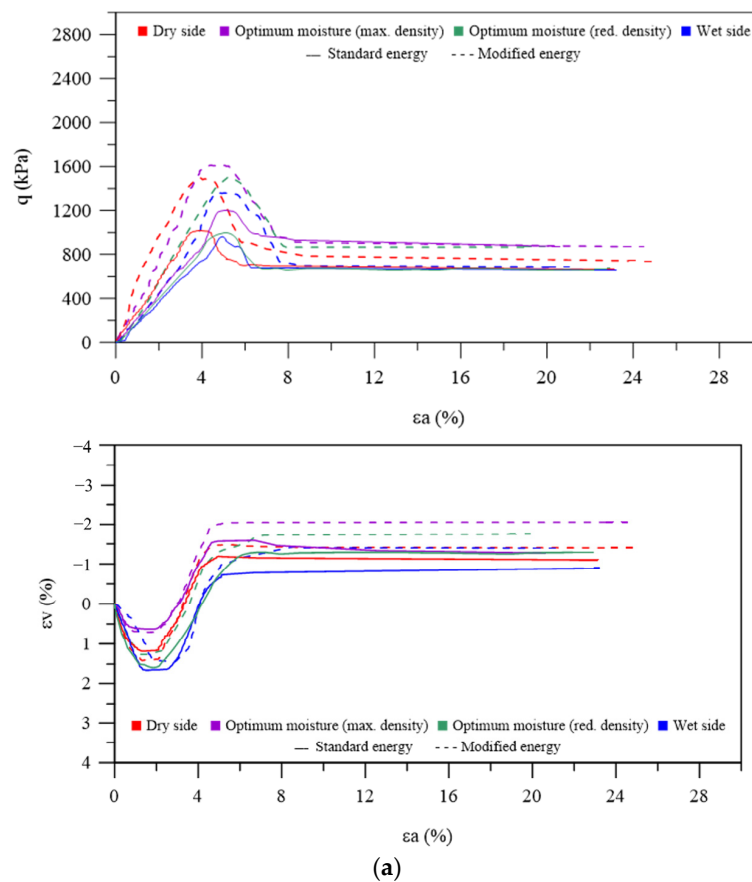
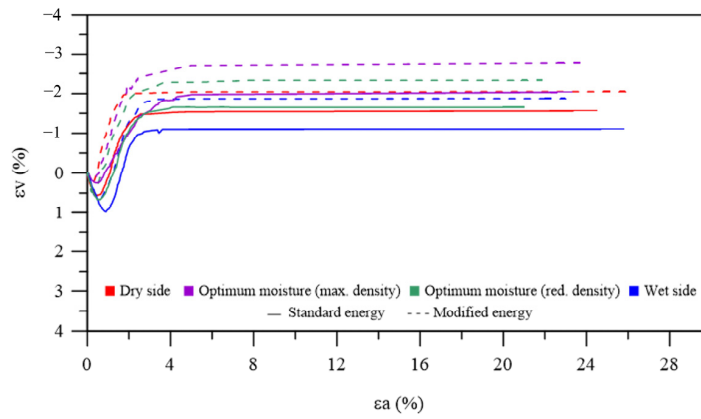
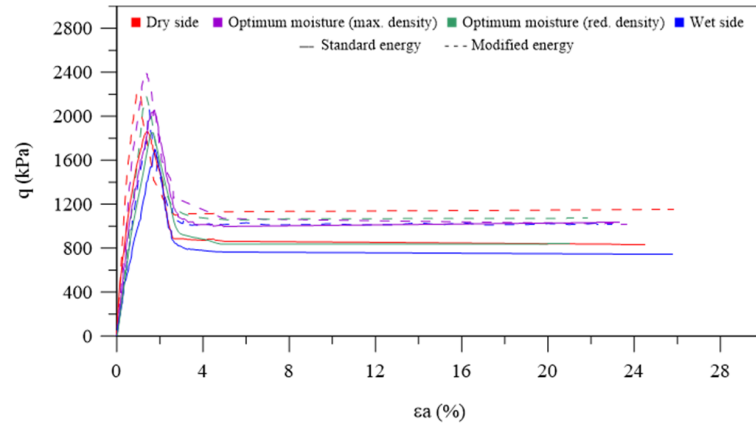
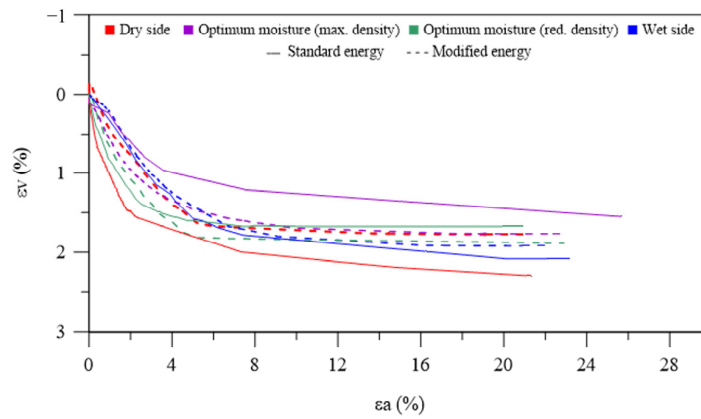
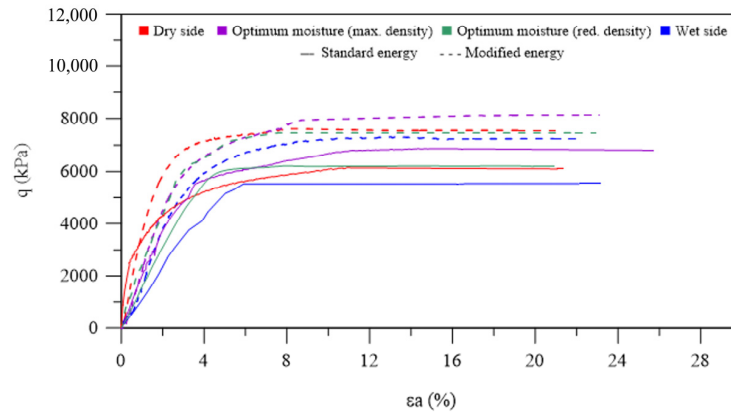


Figure 4. Cont.



(b)



(c)

Figure 4. Cont.

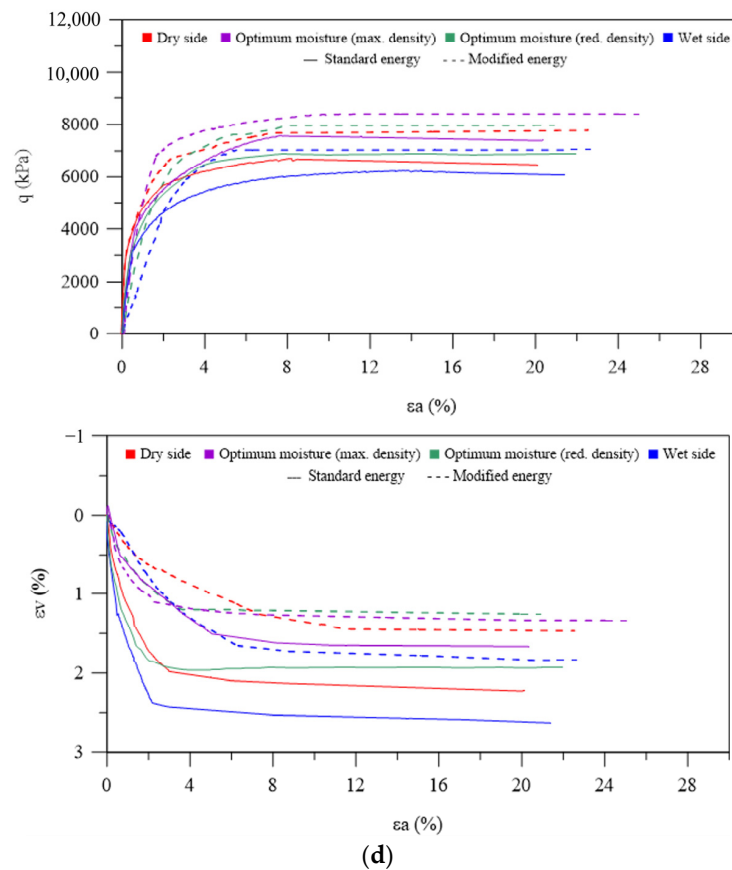


Figure 4. Triaxial stress–strain data and volume change response: (a) $p'_0 = 300$ kPa, uncemented; (b) $p'_0 = 300$ kPa, cemented; (c) $p'_0 = 3000$ kPa, uncemented; (d) $p'_0 = 3000$ kPa, cemented.

Considering the lowest confinement level, all specimens have shown an initial brittle response, presenting well-defined peak stress, followed by post-peak strain softening. This was accompanied by an initial contraction, followed by a dilatative trend. For the uncemented samples, the peak stress coincides with the highest dilation rate, which is the typical response of purely frictional granular materials. This was not the case for the cement-containing specimens [21,22]. For both cemented and uncemented samples, the top deviatoric stress (q_{max}) was proportional to the molding void ratio when considering the optimum molding conditions at standard and modified compaction efforts (i.e., γ_{dmax} and w_{opt}). Moreover, slightly higher strengths were obtained for the specimens molded at the optimum moisture content but with reduced dry unit weight, followed by the dry side samples and, ultimately, the wet side ones. The addition of cement has also led to a substantial increment in the strength and pre-peak stiffness of the samples, has augmented the dilation rate, and has enhanced the brittleness. This suggests that the cement bonds have remained intact during the consolidation phase up to the attainment of $p'_0 = 300$ kPa [23]. In other words, the cement bonds were responsible for the reported strength and stiffness gains as they only degraded during the shearing [22,49].

Concerning the highest confinement, both uncemented and cemented specimens have not presented a well-defined peak strength and have shown a fully contractive response, characterizing a ductile behavior. For most of the tests conducted at $p'_0 = 3000$ kPa, the deviatoric stress (q) and the volumetric strain (ϵ_v) seem to stabilize for axial strain (ϵ_a) values greater than 15%. Moreover, the cement addition appeared to have negligible influence on the iron ore tailings' responses to this high confinement level, indicating that the bonds were probably broken during the consolidation phase [49–51]. This is corroborated by the quantitatively and qualitatively similar responses of the cemented and uncemented samples under the highest confining stress that attained deviatoric stresses of the same order of

magnitude and comparable compression during shear. The top strength value followed the previously discussed trend for the $p'_0 = 300$ kPa tests.

Table 3. Triaxial test specimens' characteristics.

Specimen	p'_0 (kPa)	e_0	e_c	$G\varepsilon_s = 0.5\%$ (MPa)	
S_W_3C	300 kPa	0.59	0.57	56.1	
S_O_3C		0.54	0.53	63.8	
S_R_3C		0.58	0.57	68.8	
S_D_3C		0.58	0.57	76.6	
M_W_3C		0.49	0.49	63.1	
M_O_3C		0.44	0.43	75.2	
M_R_3C		0.44	0.43	83.5	
M_D_3C		0.49	0.47	88.8	
S_W_0C		0.58	0.57	7.5	
S_O_0C		0.54	0.53	9.4	
S_R_0C		0.58	0.57	11.1	
S_D_0C		0.58	0.56	15.2	
M_W_0C		0.48	0.48	21.4	
M_O_0C		0.44	0.43	9.8	
M_R_0C		0.44	0.43	11.2	
M_D_0C		0.48	0.47	38.5	
S_W_3C		3000 kPa	0.59	0.41	188.5
S_O_3C			0.54	0.43	261.5
S_R_3C	0.58		0.43	282.4	
S_D_3C	0.58		0.43	303.9	
M_W_3C	0.49		0.42	170.5	
M_O_3C	0.44		0.41	264.7	
M_R_3C	0.48		0.42	221.5	
M_D_3C	0.49		0.41	351.3	
S_W_0C	0.58		0.43	33.5	
S_O_0C	0.54		0.43	66.6	
S_R_0C	0.58		0.43	69.8	
S_D_0C	0.58		0.42	146.6	
M_W_0C	0.48		0.43	46.8	
M_O_0C	0.44		0.40	71.6	
M_R_0C	0.48		0.42	74.8	
M_D_0C	0.48		0.41	109.7	

5.2.2. Effect of Molding Characteristics

For the uncemented samples, within each confinement level and separately considering each compaction energy, the highest strength was attained at the optimum molding conditions (i.e., lowest void ratio and optimum moisture content). This reinforces the role of the degree of interlocking in the strength of purely frictional materials, which contributes to minimizing the compressive trend and assists in enhancing the strength associated with dilation, particularly for lower confinement pressures [52–54]. For the 97% compaction degree, the specimens assembled using the optimum moisture content and the dry side samples attained comparable top strength values. They were slightly less compressible and more dilatant than the wet-side ones, thus more resistant. The fabrics that have arisen when compacting the samples using lower moisture contents have favored this trend because the particles are less lubricated than in the wet-side arrangement and, as a reason, less likely to compress during shear. Considering the cemented samples, the same trend regarding the strength response was obtained, but with the addition of a cohesion-related strength parcel for the $p'_0 = 300$ kPa tests [18,21,55]. This has substantially increased the top strength in comparison to the uncemented samples.

In contrast, the initial stiffness does not follow the above trend for the strength data. For both the cemented and uncemented specimens, and within the same compaction energy, the dry-side samples were initially stiffer, followed by the ones molded at the optimum conditions, the ones compacted at the optimum moisture content but with reduced dry density, and, ultimately, the ones compacted on the wet side. This indicates that the fabric created by the compaction on the dry side of the compaction curves has favored the stiffness. The lack of lubrication between the particles on the dry side has somewhat restrained the

relative movement between the constituent grains, enhancing the stiffness in this condition. Consoli et al. [50] reported a similar trend for conventional geotechnical materials. Likewise, the cement addition enhanced the initial stiffness of the iron ore tailings, particularly in $p'_0 = 300$ kPa tests, in which the cemented samples were initially much stiffer than the uncemented ones. This difference is not as pronounced for the highest level of confinement since most of the cement bonds were broken during consolidation. The shear modulus values corroborate these for a distortional strain of $\epsilon_s = 0.5\%$, summarized in the last column of Table 3.

5.3. Particle Breakage Analysis

Figure 5 depicts the grain size distribution of the specimens submitted to the one-dimensional compression tests, and Figure 6 exhibits the same regarding the triaxial tests conducted at $p'_0 = 3000$ kPa. Both figures contain the gradation of the natural (untested) iron ore tailings. Table 4 summarizes the particle breakage factor (B_f) calculated based on those curves.

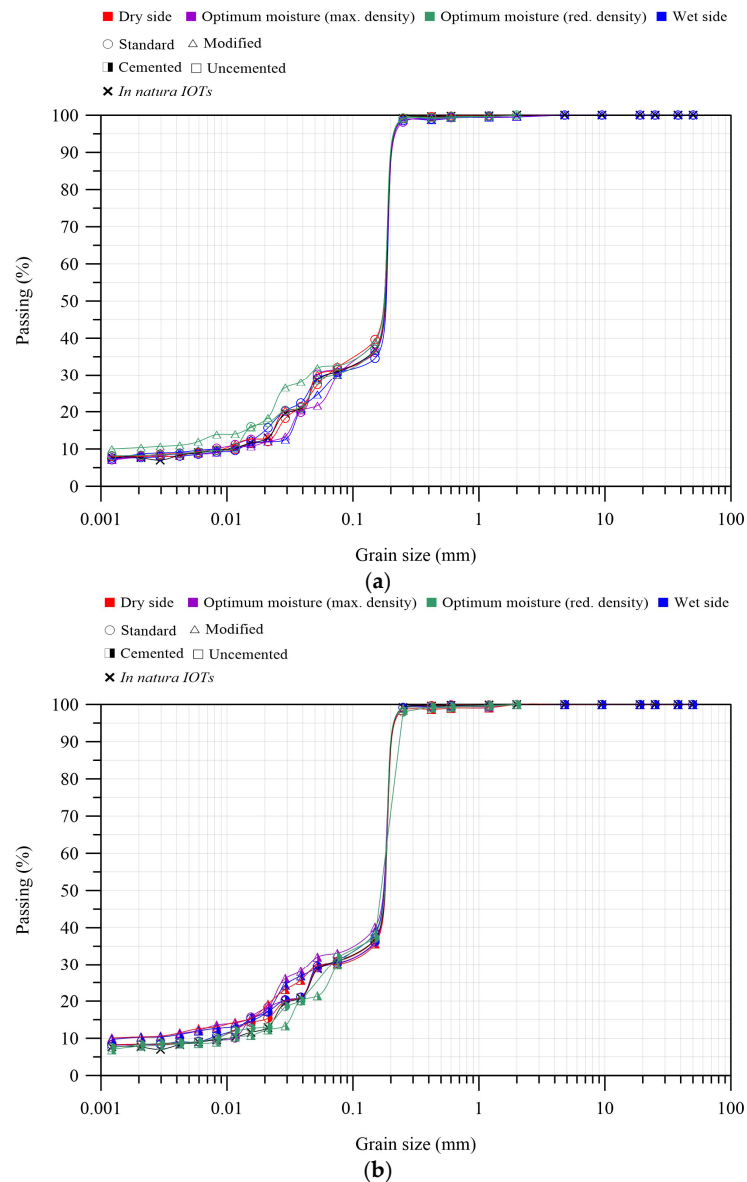


Figure 5. Grain size distribution test conducted after the one-dimensional compression test: (a) uncemented and (b) cemented.

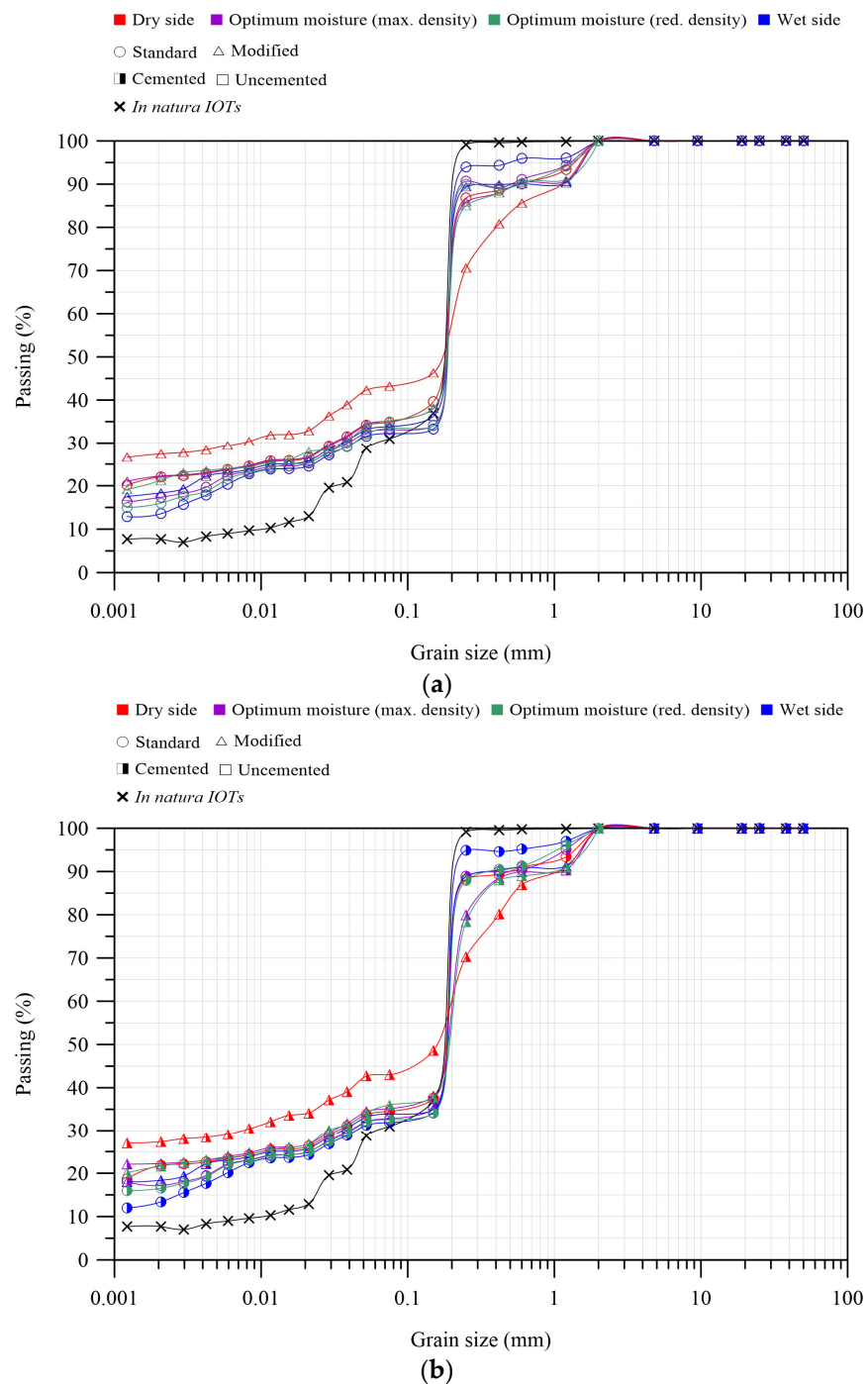
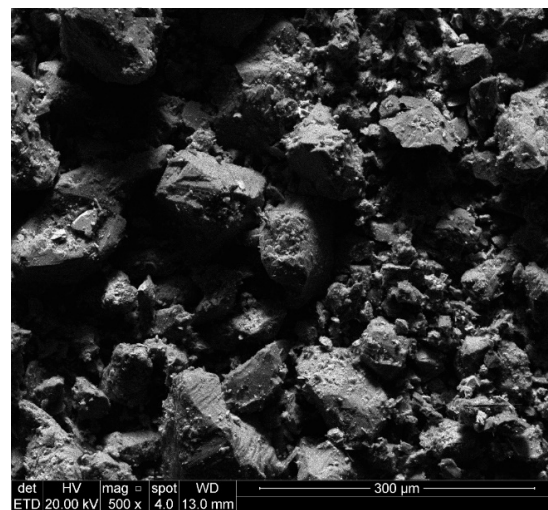


Figure 6. Grain size distribution test conducted after the triaxial test: (a) uncemented and (b) cemented.

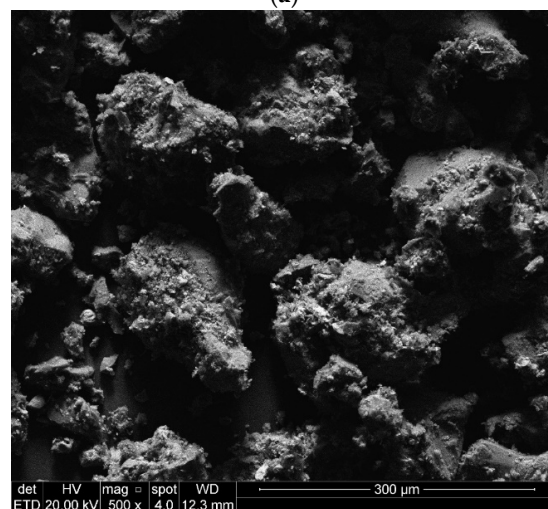
The amount of grain crushing due to one-dimensional compression is negligible, as evidenced by the near-zero values of the B_f , regardless of the specimen's characteristics. This is corroborated by the SEM micrographs of specimens M_D_3C and M_D_0C, shown in Figure 7a and 7b, respectively. Features of the tested material, such as particle size, shape, and surface roughness, have remained unaltered when vertically compressed up to 6400 kPa. Higher pressures would probably cause grain breakage for this loading condition [56,57].

Table 4. Particle breakage factor.

Specimen	Particle Breakage Factor (B_f)	
	Test Type	
	1-D Comp.	Triaxial
S_W_3C	0.02	0.04
S_O_3C	0.02	0.10
S_R_3C	0.01	0.08
S_D_3C	0.02	0.11
M_W_3C	0.01	0.10
M_O_3C	0.01	0.14
M_R_3C	0.02	0.11
M_D_3C	0.01	0.19
S_W_0C	0.00	0.05
S_O_0C	0.00	0.09
S_R_0C	0.00	0.07
S_D_0C	0.00	0.12
M_W_0C	0.00	0.10
M_O_0C	0.00	0.13
M_R_0C	0.00	0.11
M_D_0C	0.00	0.19



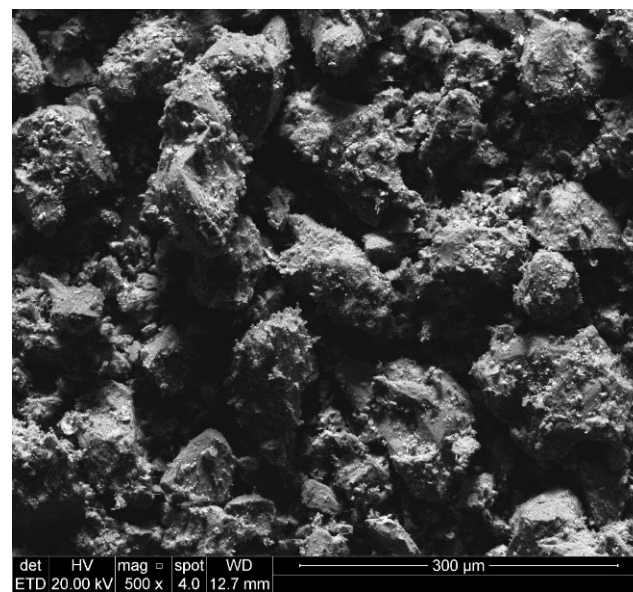
(a)



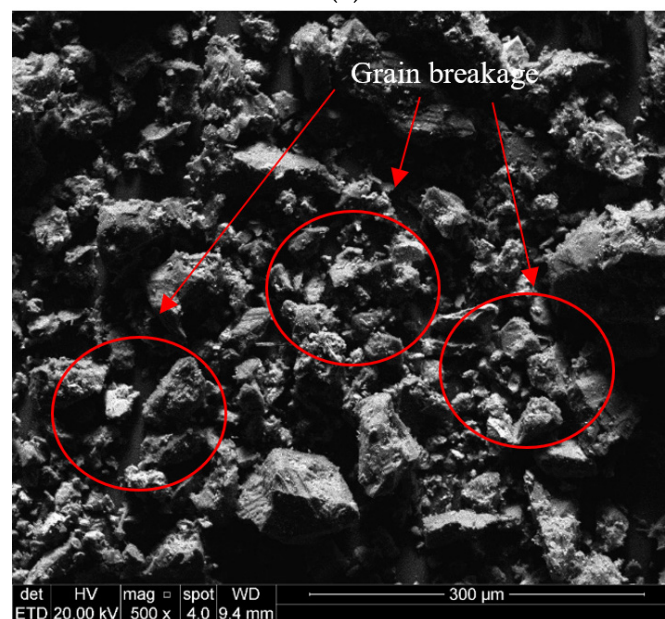
(b)

Figure 7. SEM micrographs after one-dimensional compression tests at 500× magnification rate: (a) M_D_0C and (b) M_D_3C.

In contrast, shearing at $p'_0 = 3000$ kPa caused grain breakage, which varied according to the molding specimen's characteristics, suggesting that B_f values ranged from 4% to 19%. The amount of particle crushing was higher when the specimens were molded at a modified energy (97% or 100% of compaction degree), which is probably related to the denser packing that favored inter-particle contact [58]. Considering the moisture content, the specimens compacted on the wet side presented slightly lower B_f values, which is probably related to the higher degree of lubrication between the particles in this condition. Moreover, the cement-containing specimens showed marginally higher B_f values than the uncemented samples compacted at the same density and using the same moisture content. However, this difference was practically negligible. The after-shearing SEM micrographs of samples M_D_3C and M_D_0C are presented in Figure 8a and 8b, respectively.



(a)



(b)

Figure 8. SEM micrographs after triaxial testing at 500× magnification rate: (a) M_D_0C and (b) M_D_3C. Red circles and arrows represent the grain breakage of the samples.

It is noticeable that the particles became smaller and slightly more angular owing to the breakage that occurred during shearing. Again, no differences between the cemented and uncemented samples can be noticed, indicating that the cement bonds were thoroughly broken during the 3000 kPa consolidation stage.

6. Concluding Remarks

From the data presented herein and considering the boundaries of the present research, the following conclusions can be drawn:

- Despite the non-convergent behavior of all samples up to the attained vertical stress ($\sigma'_v = 6400$ kPa), as indicated by the different compression index values between the denser and looser samples, the studied iron ore tailings appear to be non-transitional since a near-zero m parameter value was obtained. This indicates that fabric-related differences resulting from various molding conditions (such as compaction degree, initial moisture content, and cement addition) diminish at higher stress levels during one-dimensional compression.
- The molding characteristics appeared to have significantly influenced the stress–strain response of the triaxial tests considering the lowest confining pressure ($p'_0 = 300$ kPa). At the highest confinement level ($p'_0 = 3000$ kPa), most of the cement bonds were broken during the consolidation phase, exerting a marginal effect on the shearing phase.
- For lower confinement levels, the cement addition appears to be an interesting option to enhance the strength and stiffness of the compacted iron ore tailings. Compacting the samples at the optimum conditions maximizes the top strength. In contrast, the initial stiffness is enhanced when the compaction is performed on the dry side of the compaction curve.
- The one-dimensional compression tests did not reveal substantial particle breakage, regardless of the initial molding characteristics. On the other side, shearing at $p'_0 = 3000$ kPa generated a considerable grain breakage, particularly in the densest samples. In this regard, the cement addition appeared to have exerted a marginal influence concerning preventing particle breakage due to shearing at $p'_0 = 3000$ kPa.
- Despite the differences arising from using distinct compaction characteristics, the overall volume change response was not profoundly altered by adding cement and altering the molding moisture content. In other words, all the specimens sheared at $p'_0 = 300$ kPa initially contracted and then dilated, whereas all the specimens sheared at $p'_0 = 3000$ kPa contracted.
- The durability of artificially cemented filtered iron ore tailings is relevant for adequately designing and maintaining dry stacking facilities. Particularly those submitted to harsh environmental conditions. Therefore, it is an exciting topic for future research.

Author Contributions: Conceptualization, G.J.B., H.C.S.F. and N.C.C.; methodology, G.J.B., C.P.D.S., H.C.S.F., C.d.S.M., L.R.S., J.P.d.S.S. and N.C.C.; validation, G.J.B. and H.C.S.F.; formal analysis, G.J.B., C.P.D.S., H.C.S.F., C.d.S.M. and L.R.S.; investigation, G.J.B., C.P.D.S., H.C.S.F., C.d.S.M. and L.R.S.; resources, J.P.d.S.S. and N.C.C.; data curation, G.J.B. and H.C.S.F.; writing—original draft preparation, G.J.B. and H.C.S.F.; writing—review and editing, G.J.B., C.P.D.S., H.C.S.F., C.d.S.M., L.R.S., J.P.d.S.S. and N.C.C.; visualization, J.P.d.S.S. and N.C.C.; supervision, N.C.C.; project administration, N.C.C. All authors have read and agreed to the published version of the manuscript.

Funding: This research received no external funding.

Data Availability Statement: Some or all data, models, or codes that support the findings of this study are available from the corresponding author upon reasonable request.

Acknowledgments: The authors wish to express their appreciation for VALE S.A. and the Brazilian Research Council (CNPq) for supporting the research group.

Conflicts of Interest: João Paulo de Souza Silva employed by the company VALE S.A. The remaining authors declare that the research was conducted in the absence of any commercial or financial relationships that could be construed as a potential conflict of interest.

Notations

γ_d	dry unit weight
γ_s	unit weight of solids of the iron ore tailings
w	moisture content
G	initial shear modulus
γ	bulk density
1-D	one-dimensional
CID	consolidated isotropically drained
SEM	scanning electron microscope
XRD	X-ray diffraction
XRF	X-ray fluorescence
IOT	iron ore tailings
NCL	normal compression line
M	modified compaction energy
S	standard compaction energy
W	wet side
D	dry side
O	optimum molding conditions
e_0	molding void ratio
e_c	after consolidation, the void ratio
B_f	breakage factor
C	amount of cement expressed in percentage
C_c	compression index
p'	mean effective stress
p'_0	initial mean effective stress
q	deviatoric stress
q_{max}	peak deviatoric stress
ϵ_a	axial strain
ϵ_v	volumetric strain
ϵ_s	distortional strain
σ'_v	vertical stress
σ_1, σ_3	principal stresses

References

1. Cacciuttolo Vargas, C.; Pérez Campomanes, G. Practical Experience of Filtered Tailings Technology in Chile and Peru: An Environmentally Friendly Solution. *Minerals* **2022**, *12*, 889. [[CrossRef](#)]
2. Gomes, R.B.; De Tomi, G.; Assis, P.S. Iron Ore Tailings Dry Stacking in Pau Branco Mine, Brazil. *J. Mater. Res. Technol.* **2016**, *5*, 339–344. [[CrossRef](#)]
3. Bedin, J.; Schnaid, F.; Da Fonseca, A.V.; Costa Filho, L.D.M. Gold Tailings Liquefaction under Critical State Soil Mechanics. *Géotechnique* **2012**, *62*, 263–267. [[CrossRef](#)]
4. Carrera, A.; Coop, M.; Lancellotta, R. Influence of Grading on the Mechanical Behaviour of Stava Tailings. *Géotechnique* **2011**, *61*, 935–946. [[CrossRef](#)]
5. Oldecop, L.; Rodari, G. Unsaturated Mine Tailings Disposal. *Soils Rocks* **2021**, *44*, 1–12. [[CrossRef](#)]
6. Schaper, D.; Lessa, R.; Freitas, A.; Weeks, B. De-Characterization and Closure of TSF: Concepts of the Brazilian Legislation and International Criteria. *Plan. Clos.* **2020**, *3*.
7. Armstrong, M.; Petter, R.; Petter, C. Why Have so Many Tailings Dams Failed in Recent Years? *Resour. Policy* **2019**, *63*, 101412. [[CrossRef](#)]
8. Islam, K.; Murakami, S. Global-Scale Impact Analysis of Mine Tailings Dam Failures: 1915–2020. *Glob. Environ. Chang.* **2021**, *70*, 102361. [[CrossRef](#)]
9. Lyu, Z.; Chai, J.; Xu, Z.; Qin, Y.; Cao, J. A Comprehensive Review on Reasons for Tailings Dam Failures Based on Case History. *Adv. Civ. Eng.* **2019**, *2019*, 4159306. [[CrossRef](#)]
10. Dauce, P.D.; De Castro, G.B.; Lima, M.M.F.; Lima, R.M.F. Characterisation and Magnetic Concentration of an Iron Ore Tailings. *J. Mater. Res. Technol.* **2019**, *8*, 1052–1059. [[CrossRef](#)]
11. Vilaça, A.S.I.; Simão, L.; Montedo, O.R.K.; Novaes de Oliveira, A.P.; Raupp-Pereira, F. Waste Valorization of Iron Ore Tailings in Brazil: Assessment Metrics from a Circular Economy Perspective. *Resour. Policy* **2022**, *75*, 102477. [[CrossRef](#)]
12. Kossoff, D.; Dubbin, W.E.; Alfredsson, M.; Edwards, S.J.; Macklin, M.G.; Hudson-Edwards, K.A. Mine Tailings Dams: Characteristics, Failure, Environmental Impacts, and Remediation. *Appl. Geochem.* **2014**, *51*, 229–245. [[CrossRef](#)]
13. Santamarina, J.C.; Torres-Cruz, L.A.; Bachus, R.C. Why Coal Ash and Tailings Dam Disasters Occur. *Science* **2019**, *364*, 526–528. [[CrossRef](#)] [[PubMed](#)]
14. Ahmed, S.I.; Siddiqua, S.; Renner, S. Development of a Model to Predict Consolidation of Tailings. *Environ. Geotech.* **2018**, *5*, 271–284. [[CrossRef](#)]
15. Ledesma, O.; Sfriso, A.; Manzanal, D. Procedure for Assessing the Liquefaction Vulnerability of Tailings Dams. *Comput. Geotech.* **2022**, *144*, 104632. [[CrossRef](#)]

16. Bruschi, G.J.; Dos Santos, C.P.; Tonini de Araújo, M.; Ferrazzo, S.T.; Marques, S.F.V.; Consoli, N.C. Green Stabilization of Bauxite Tailings: Mechanical Study on Alkali-Activated Materials. *J. Mater. Civ. Eng.* **2021**, *33*, 06021007. [[CrossRef](#)]
17. Consoli, N.C.; Da Silva, A.P.; Nierwinski, H.P.; Sosnoski, J. Durability, Strength, and Stiffness of Compacted Gold Tailings—Cement Mixes. *Can. Geotech. J.* **2018**, *55*, 486–494. [[CrossRef](#)]
18. Consoli, N.C.; Vogt, J.C.; Silva, J.P.S.; Chaves, H.M.; Scheuermann Filho, H.C.; Moreira, E.B.; Lotero, A. Behaviour of Compacted Filtered Iron Ore Tailings–Portland Cement Blends: New Brazilian Trend for Tailings Disposal by Stacking. *Appl. Sci.* **2022**, *12*, 836. [[CrossRef](#)]
19. Festugato, L.; Fourie, A.; Consoli, N.C. Cyclic Shear Response of Fibre-Reinforced Cemented Paste Backfill. *Géotech. Lett.* **2013**, *3*, 5–12. [[CrossRef](#)]
20. Pereira dos Santos, C.; Bruschi, G.J.; Mattos, J.R.G.; Consoli, N.C. Stabilization of Gold Mining Tailings with Alkali-Activated Carbide Lime and Sugarcane Bagasse Ash. *Transp. Geotech.* **2022**, *32*, 100704. [[CrossRef](#)]
21. Schnaid, F.; Prietto, P.D.M.; Consoli, N.C. Characterization of Cemented Sand in Triaxial Compression. *J. Geotech. Geoenviron. Eng.* **2001**, *127*, 857–868. [[CrossRef](#)]
22. Lade, P.V.; Trads, N. The Role of Cementation in the Behaviour of Cemented Soils. *Geotech. Res.* **2014**, *1*, 111–132. [[CrossRef](#)]
23. Rotta, G.V.; Consoli, N.C.; Prietto, P.D.M.; Coop, M.R.; Graham, J. Isotropic Yielding in an Artificially Cemented Soil Cured under Stress. *Géotechnique* **2003**, *53*, 493–501. [[CrossRef](#)]
24. Behera, S.; Mishra, D.; Singh, P.; Mishra, K.; Mandal, S.K.; Ghosh, C.; Kumar, R.; Mandal, P.K. Utilization of mill tailings, fly ash and slag as mine paste backfill material: Review and future perspective. *Constr. Build. Mater.* **2021**, *309*, 120–125. [[CrossRef](#)]
25. Ercikdi, B.; Cihangir, F.; Kesimal, A.; Deveci, H. Practical Importance of Tailings for Cemented Paste Backfill. In *Paste Tailings Management*; Yilmaz, E., Fall, M., Eds.; Springer International Publishing: Cham, Switzerland, 2017; pp. 7–32, ISBN 978-3-319-39680-4.
26. Jiang, H.; Fall, M. Yield stress and strength of saline cemented tailings in sub-zero environments: Portland cement paste backfill. *Int. J. Miner. Process.* **2017**, *160*, 68–75. [[CrossRef](#)]
27. Kasap, T.; Yilmaz, E.; Guner, N.U.; Sari, M. Recycling Dam Tailings as Cemented Mine Backfill: Mechanical and Geotechnical Properties. *Adv. Mater. Sci. Eng.* **2022**, *2022*, 6993068. [[CrossRef](#)]
28. Mitchell, R.J.; Olsen, R.S.; Smith, J.D.; Li, L.; Aubertin, M.; Thompson, B.; Bawden, W.; Grabinsky, M. Model studies on cemented tailings used in mine backfill. *Can. Geotech. J.* **1982**, *19*, 14–28. [[CrossRef](#)]
29. Qi, C.; Fourie, A. Cemented paste backfill for mineral tailings management: Review and future perspectives. *Miner. Eng.* **2019**, *144*, 106025. [[CrossRef](#)]
30. *ASTM D7928*; Test Method for Particle-Size Distribution (Gradation) of Fine-Grained Soils Using the Sedimentation (Hydrometer) Analysis. ASTM International: West Conshohocken, PA, USA, 2021.
31. *ASTM D4318*; Test Methods for Liquid Limit, Plastic Limit, and Plasticity Index of Soils. ASTM International: West Conshohocken, PA, USA, 2017.
32. *ASTM D854*; Test Methods for Specific Gravity of Soil Solids by Water Pycnometer. ASTM International: West Conshohocken, PA, USA, 2014.
33. *ASTM D2487*; Practice for Classification of Soils for Engineering Purposes (Unified Soil Classification System). ASTM International: West Conshohocken, PA, USA, 2017.
34. *ASTM D698*; Test Methods for Laboratory Compaction Characteristics of Soil Using Standard Effort (12,400 Ft-Lbf/Ft³ (600 KN-m/M<sup>3- 35. *ASTM D1557*; Test Methods for Laboratory Compaction Characteristics of Soil Using Modified Effort (56,000 Ft-Lbf/Ft³ (2700 KN-m/M<sup>3- 36. Carmignano, O.; Vieira, S.; Teixeira, A.P.; Lameiras, F.; Brandão, P.R.; Lago, R. Iron Ore Tailings: Characterization and Applications. *J. Braz. Chem. Soc.* **2021**, *32*, 1895–1911. [[CrossRef](#)]
- 37. Chang, N.; Heymann, G.; Clayton, C. The Effect of Fabric on the Behaviour of Gold Tailings. *Géotechnique* **2011**, *61*, 187–197. [[CrossRef](#)]
- 38. Nie, W.; Li, C.; Hu, J.; Saffari, P.; Wang, W.; Luo, M. Spatial Variation of Physical and Mechanical Properties of Tailings under Different Rainfall Intensities and the Interaction Pattern. *Geomech. Geophys. Geo-Energy Geo-Resour.* **2023**, *9*, 86. [[CrossRef](#)]
- 39. Li, Y.; Otsubo, M.; Kuwano, R. Evaluation of Soil Fabric Using Elastic Waves during Load-Unload. *J. Rock Mech. Geotech. Eng.* **2023**, *15*, 2687–2700. [[CrossRef](#)]
- 40. Shaker, A.A.; Elkady, T.Y. Hydraulic Performance of Sand–Clay Mixtures: Soil Fabric Perspective. *Géotech. Lett.* **2015**, *5*, 198–204. [[CrossRef](#)]
- 41. Yimsiri, S.; Soga, K. Effects of Soil Fabric on Behaviors of Granular Soils: Microscopic Modeling. *Comput. Geotech.* **2011**, *38*, 861–874. [[CrossRef](#)]
- 42. *ASTM D2435*; Test Methods for One-Dimensional Consolidation Properties of Soils Using Incremental Loading. ASTM International: West Conshohocken, PA, USA, 2011.
- 43. *ASTM D7181*; Test Method for Consolidated Drained Triaxial Compression Test for Soils. ASTM International: West Conshohocken, PA, USA, 2020.
- 44. Clayton, C.R.I.; Khattrush, S.A. A New Device for Measuring Local Axial Strains on Triaxial Specimens. *Géotechnique* **1986**, *36*, 593–597. [[CrossRef](#)]</sup></sup>

45. Nakata, A.F.L.; Hyde, M.; Hyodo, H.; Murata. A Probabilistic Approach to Sand Particle Crushing in the Triaxial Test. *Géotechnique* **1999**, *49*, 567–583. [[CrossRef](#)]
46. Li, W.; Coop, M.R. Mechanical Behaviour of Panzhihua Iron Tailings. *Can. Geotech. J.* **2019**, *56*, 420–435. [[CrossRef](#)]
47. Ponzoni, E.; Nocilla, A.; Coop, M.R.; Colleselli, F. Identification and Quantification of Transitional Modes of Behaviour in Sediments of Venice Lagoon. *Géotechnique* **2014**, *64*, 694–708. [[CrossRef](#)]
48. Todisco, M.C.; Coop, M.R. Quantifying “Transitional” Soil Behaviour. *Soils Found.* **2019**, *59*, 2070–2082. [[CrossRef](#)]
49. Malandraki, V.; Toll, D. Drained Probing Triaxial Tests on a Weakly Bonded Artificial Soil. *Géotechnique* **2000**, *50*, 141–151. [[CrossRef](#)]
50. Alvarado, G.; Coop, M.R.; Willson, S. On the Role of Bond Breakage Due to Unloading in the Behaviour of Weak Sandstones. *Géotechnique* **2012**, *62*, 303–316. [[CrossRef](#)]
51. Alvarado, G.; Lui, N.; Coop, M.R. Effect of Fabric on the Behaviour of Reservoir Sandstones. *Can. Geotech. J.* **2012**, *49*, 1036–1051. [[CrossRef](#)]
52. Reza Fotovvat, A.; Sadrekarimi, A. Instability of a Gold Mine Tailings Subjected to Different Stress Paths. *J. Geotech. Geoenviron. Eng.* **2022**, *148*, 04022020. [[CrossRef](#)]
53. Salvatore, E.; Modoni, G.; Andò, E.; Albano, M.; Viggiani, G. Determination of the Critical State of Granular Materials with Triaxial Tests. *Soils Found.* **2017**, *57*, 733–744. [[CrossRef](#)]
54. Wagner, A.C.; De Sousa Silva, J.P.; De Azambuja Carvalho, J.V.; Cezar Rissoli, A.L.; Cacciari, P.P.; Chaves, H.M.; Scheuermann Filho, H.C.; Consoli, N.C. Mechanical Behavior of Iron Ore Tailings under Standard Compression and Extension Triaxial Stress Paths. *J. Rock Mech. Geotech. Eng.* **2023**, *15*, 1883–1894. [[CrossRef](#)]
55. Lade, P.V.; Overton, D.D. Cementation Effects in Frictional Materials. *J. Geotech. Eng.* **1989**, *115*, 1373–1387. [[CrossRef](#)]
56. Kikumoto, M.; Wood, D.M.; Russell, A. Particle Crushing and Deformation Behaviour. *Soils Found.* **2010**, *50*, 547–563. [[CrossRef](#)]
57. Zhang, T.; Yang, W.; Zhang, C.; Hu, C. Particle Breakage Effect on Compression Behavior of Realistic Granular Assembly. *Int. J. Geomech.* **2021**, *21*, 04021105. [[CrossRef](#)]
58. Wei, H.; Li, X.; Zhang, S.; Zhao, T.; Yin, M.; Meng, Q. Influence of Particle Breakage on Drained Shear Strength of Calcareous Sands. *Int. J. Geomech.* **2021**, *21*, 04021118. [[CrossRef](#)]

Disclaimer/Publisher’s Note: The statements, opinions and data contained in all publications are solely those of the individual author(s) and contributor(s) and not of MDPI and/or the editor(s). MDPI and/or the editor(s) disclaim responsibility for any injury to people or property resulting from any ideas, methods, instructions or products referred to in the content.